Title:

Modeling Lithospheric Radioactivity Influence on Atmospheric Electric Properties Relative to Earthquakes

Authors:
Ahmad Muhammad[1]*, Fatma Almaz[2], Fatih Külahcı[3]
[1] Qatar University, College of Arts and Sciences, Department of Physics and Materials Sciences, Doha, Qatar
[2] Batman University, Faculty of Science and Letters, Department of Mathematics, Batman, Türkiye
[3] ASELSAN Electronic Industry and Trade Joint Stock Company, Ankara, Türkiye

Corresponding author:
Ahmad Muhammad (ahmadmuhammad325@gmail.com, a.muhammad@qu.edu.qa)

Corresponding author ORCID: https://orcid.org/0000-0003-3886-7956

Modeling Lithospheric Radioactivity Influence on Atmospheric Electric Properties relative to Earthquakes

Ahmad Muhammad[1]*, Fatma Almaz[2], Fatih Külahcı[3]

[1]Qatar University, College of Arts and Sciences, Department Physics and Materials Sciences, 2713, Doha, Qatar

[2]Batman University, Faculty of Science and Letters, Department of Mathematics, Batman, Türkiye

[3]ASELSAN Electronic Industry and Trade Joint Stock Company, TR-06200, Ankara, Türkiye

*Corresponding author. Tel:

Emails: a.muhammad@qu.edu.qa*;ahmadmuhammad325@gmail.com

Abstract

This study presents a mathematical exploration of the atmospheric electric field components resulting from radon-induced ionization, with implications in the study of earthquake phenomena. By formalizing the general solution to the proposed equations with given boundary conditions, the research offers a comparative analysis of electric parameters across different radon concentrations and radii of influence. The near-surface atmospheric electric field and electric potential are found to vary within the ranges of $(1-27)\,V/m$ and $(0.3-162)\,V$ respectively, while near-surface conductivity varies between $(1-29)\times 10^{-14} Sm^{-1}$. The study highlights the sensitivity of boundary layer conductivity to radon exhalation and discusses the indirect relationship between radon and the upper atmosphere in the context of the Global Electric Circuit (GEC) and earthquake. The behavior of radon-induced electric fields and potentials from the surface to upper atmospheric heights is analyzed, particularly in relation to seismic activity. The role of local atmospheric conditions as amplifiers or dampeners of radon's influence is also explored. The tabulated data provide reference values for real-world observations, demonstrating the dominant influence of radon on electric parameters at lower altitudes and their attenuation at ionospheric heights. The potential geophysical interplay between radon emanations and seismic activities is suggested, highlighting the need for further investigation into this complex relationship to enhance earthquake prediction.

Key words: Radon, earthquake, atmospheric electric field

1. Introduction

A majority of natural disasters like earthquakes, hurricane, volcanic activities, Tsunamis etc. happen as a consequential effect of the physical processes occurring either in the lithosphere or in the atmosphere. A common factor related to most disasters having lithospheric origin is earthquake (Engineering, 2018; Ersoy & Koçak, 2016; Kanamori, 1972; Walter & Amelung, 2006). However, earthquake, like most disasters, is difficult to predict. In this regard, scientists work tirelessly in order to study/understand the physical mechanisms associated with its occurrence. One of the important factors in this study is the way Earth's Lithosphere and Atmosphere or Lithosphere, Atmosphere, and Upper atmosphere (Ionosphere) are related. This is often referred to as Lithosphere-Atmosphere coupling (LA) or Lithosphere-Atmosphere-Ionosphere coupling (LAIC)(Havemann et al., 2023; Muhammad et al., 2023; Sorokin & Hayakawa, 2013). Understanding this would be of great significance in interpreting events relative to earthquakes.

Atmospheric electric field phenomenon is a topic of interest in LAIC coupling studies due to its relationship with earthquakes. It involves the study of electric field present in the Earth's atmosphere, which can be influenced by numerous factors including solar activity and tropospheric variables. Studies showed that electric fields over seismically active regions can be noticed from several minutes to days of pre or post occurrence of the main shock (Sorokin and Ruzhin, 2015). The production/dispersion of ions under the influence of earthquakes can cause changes in atmospheric electric properties within the vicinity of earthquake pre- or post-seismic regions. In recent years, researchers developed models that aim to set up relationships between the atmosphere and ionosphere (Denisenko et al., 2013; Denisenko et al., 2019; Prokhorov and Zolotov, 2017; Sorokin and Ruzhin, 2015; Zhou et al., 2017). They solve a set of equations which include the Faraday law (relating electromagnetic induction), the charge conservation law (relating the flow of charged particles), and Ohm's law (relating current and electric fields). These equations aid to uncover theoretical exchange between the near boundary layer atmospheric processes, and the ionosphere. The findings have practical implications in atmospheric science, geophysics, space weather forecasting, earthquake studies, and climate research. Some of the deductions of such studies in the LAIC (earthquake) context are presented in Table 1. The magnitude of electric field reaching ionospheric heights over a disturbed/active earthquake region is of the order between 10^{-3} and $10^{-6}\, V/m$ (Valery M. Sorokin et al., 2020) . This corresponds to an amplitude of outgoing electric field of about $E_0 = 100\, V/m$ or greater near the disturbed earth's surface region. Estimation results vary depending on model formulation assumptions, the nature of the source region, as well as the source of the generated electric field. The treatment given to lower atmospheric processes in developing such models is by adopting some literature boundary layer atmospheric electric field/conductivity amplitudes. These adopted values are then applied to serve as boundary layer values which originated from the lithosphere. In this regard, the role of lithospheric physical processes is limited.

The pursuit for a comprehensive LAIC model that considers parameters relatively common to the three spheres (lithosphere, atmosphere, and ionosphere) is inevitable. This is because, such models would enable the opportunity to explore simultaneously the feedback between Lithosphere-Atmosphere or Lithosphere-Atmosphere-Ionosphere processes in pre or post-earthquake periods. A parameter that can be promising is the radioactive radon gas. Although its relationship with the upper atmosphere is indirect (Mohammed et al., 2021), it is a common entity to both lithosphere and atmosphere. Radon is also one of the prominent sources of ionization in the lower atmosphere. Its contribution to the modification of lower atmospheric electrical properties can locally affect the electric potential existing between lower and upper atmosphere (Sorokin and Ruzhin, 2015)(Muhammad et al., 2024). This is in addition to its applications in many disciplines, especially in earthquake precursory studies(Muhammad et al., 2020; Pulinets et al., 1999).

Thus, incorporating radon in an earthquake related model would give an improved theoretical and a more comprehensive exploration of the LAIC phenomenon. This study aims to incorporate lithospheric radon influence into the LAIC model. The resulting model is used to analyze radon's influence on boundary layer atmospheric electric properties relative to earthquakes. Sensitivity analysis is applied to find how the effect or radius of earthquake preparation radius affects the generated radon induced electric field. The journey of this electric field in higher altitudes is examined. In Section 2, model formulation and boundary conditions are discussed, and the solution of theoretical LAIC coupling model is set up. In Section 3, model estimation results are presented and discussed. In the concluding section, remarks are given.

Table 1: Atmosphere-ionosphere electric properties reported by different studies, as well as the surface distribution functions.

Study	E (0,0)	Surface Rn concentration C_{Rn}	E (x, zup) max	E (0, zup)	j(x,0)

Denisenko et al., 2008	100V/m		0.1 μV/m day (10 S)	1μV/m night (0.1 S)	9 μV/m	2 μ A/m
Xu et al., 2015		30 Bqm^{-3}	0.32 μV/m day (10 S)	10μV/m night (0.1 S)		
Ampferer et al., 2010	100 V/m		0.02μV/m day (10 S)	1.9 μV/m night (0.1 S)	9.3μ V/m	0.1×10^{-7} (r=400 km) to 1×10^{-9} (r=10km) Am^{-1}
Zhou et al., 2017	1000 V/m				1 μ to 0.1 μ V/m	4 ×10^{-11} A/m
Sorokin and Ruzhin, 2015	100 V/m		10 mV/m			

1.1 Novelty and Methodological contribution

Most existing lithosphere–atmosphere–ionosphere coupling (LAIC) models prescribe near-surface electric fields, currents, or conductivities phenomenologically and treat them as external boundary conditions originating from the lithosphere. In contrast, the present study explicitly derives the lower atmospheric electric boundary conditions from lithospheric radon exhalation through a closed physical chain linking radon transport, ionization production, ion density, atmospheric conductivity, and the resulting electric field. This formulation provides a physically consistent parameterization of the boundary layer that reduces reliance on assumed surface electric amplitudes and allows systematic investigation of how radon concentration and preparation-zone radius control the vertical penetration of electric fields toward ionospheric heights. As such, the novelty of this work lies not in the governing LAIC equations themselves, which are well established, but in the explicit coupling of lithospheric radioactivity to atmospheric electric parameters used as inputs to LAIC modeling.

2.1 LAIC Model Equations

In earthquake regions, the lower and upper atmosphere can be studied by solving the Faraday's Law (Eq 1), The charge conservation law (Eq 2), and Ohm's Law (Eq 3) (Sorokin and Yaschenko, 2000).

$$\vec{\nabla} \times \vec{E} = 0 \; ; \; \vec{E} = -\vec{\nabla}\phi \qquad (1)$$

$$\vec{\nabla} \cdot \vec{J} = 0 \qquad (2)$$

$$\vec{J} = \sigma \vec{E} \qquad (3)$$

where $\vec{J}$ is the current density, $\vec{E}$ is the electrostatic field existing between the Earth's surface and upper atmospheric heights, σ is the conductivity tensor, assumed to be isotropic below ionospheric heights, and finally ϕ is the electric potential. The above three equations are represented as follows.

$$\sigma\frac{\partial^2\phi}{\partial y^2} + \sigma\frac{\partial^2\phi}{\partial x^2} + \sigma\frac{\partial^2\phi}{\partial z^2} + \frac{\partial\sigma}{\partial y}\frac{\partial\phi}{\partial y} + \frac{\partial\sigma}{\partial x}\frac{\partial\phi}{\partial x} + \frac{\partial\sigma}{\partial z}\frac{\partial\phi}{\partial z} = 0 \qquad (4)$$

The conductivity tensor σ is assumed to be isotropic in near ionospheric heights, its vertical variations would dominate, ($\frac{\partial\sigma}{\partial x} = 0$). An approximation of atmospheric conductivity tensor as a height dependent function ($\sigma = \sigma(z)$) is defined in Eq (5) (Denisenko and Boudjada, et al., 2008; Prokhorov et al., 2019; Zhou et al., 2017).

$$\sigma = \sigma_o \exp(z/h) \qquad (5)$$

where, σ_o is the near surface atmospheric electric conductivity, the estimate for this value will later be discussed. Using equation (5), it is possible to rewrite $\frac{\partial\sigma}{\partial z} = \sigma_z$ in Eq (8) such that; $\sigma_z = \frac{\sigma}{h}$. h is best referred to as conductivity scale height, it has a typical value of 6km. The solution to Eq (4) using separation of variables gives.

$$\phi(x,z) = C_1\cos(\sqrt{\mu}x) + C_2\sin(\sqrt{\mu}x)(C_3\exp(m_1 z) + C_4\exp(m_2 z)) \quad (6)$$

$m_{1,2} = -\frac{\sigma_z}{2\sigma} \pm \frac{1}{2}\sqrt{\frac{\sigma_z}{\sigma} + 4\mu}$, and C_1, C_2, C_3, C_4, μ are estimated using the boundary conditions which will follow.

2.2 Upper Boundary conditions

The geometry of the problem is presented in Figure 1. Earth's magnetic field is assumed to orient at $(I = 90^o)$ parallel to the vertical part of electric field reaching the ionosphere from earthquake region on Earth's surface (Denisenko and Boudjada, et al., 2008; Chree, C. (1913)). The upper boundary is set at Ionospheric heights $z \approx 80km$, at this region the boundary condition is defined in Eq (7a) (Denisenko and Boudjada, et al., 2008; Xu et al., 2015a).

$$\frac{-\partial}{\partial x}(\sigma_p \frac{\partial \phi}{\partial x})|_{z=z_{up}} = \sigma(z_{up})\frac{\partial \phi}{\partial z}|_{z=z_{up}} \quad (7a)$$

The ionospheric thin-layer hypothesis relies on the use of the integrated Pedersen conductivity(σ_p). σ_p has a value of about 10 S during the day, and 0.1 S at night. For simplicity, a single constant value is employed in the hypothesis. These values are taken at the upper boundary of 80 km. The reason for using a constant value of σ_p is that the horizontal scale of interest is much smaller compared to the horizontal scale of the entire ionosphere. $\sigma(z_{up})$ is the value of atmospheric conductivity at the upper boundary.

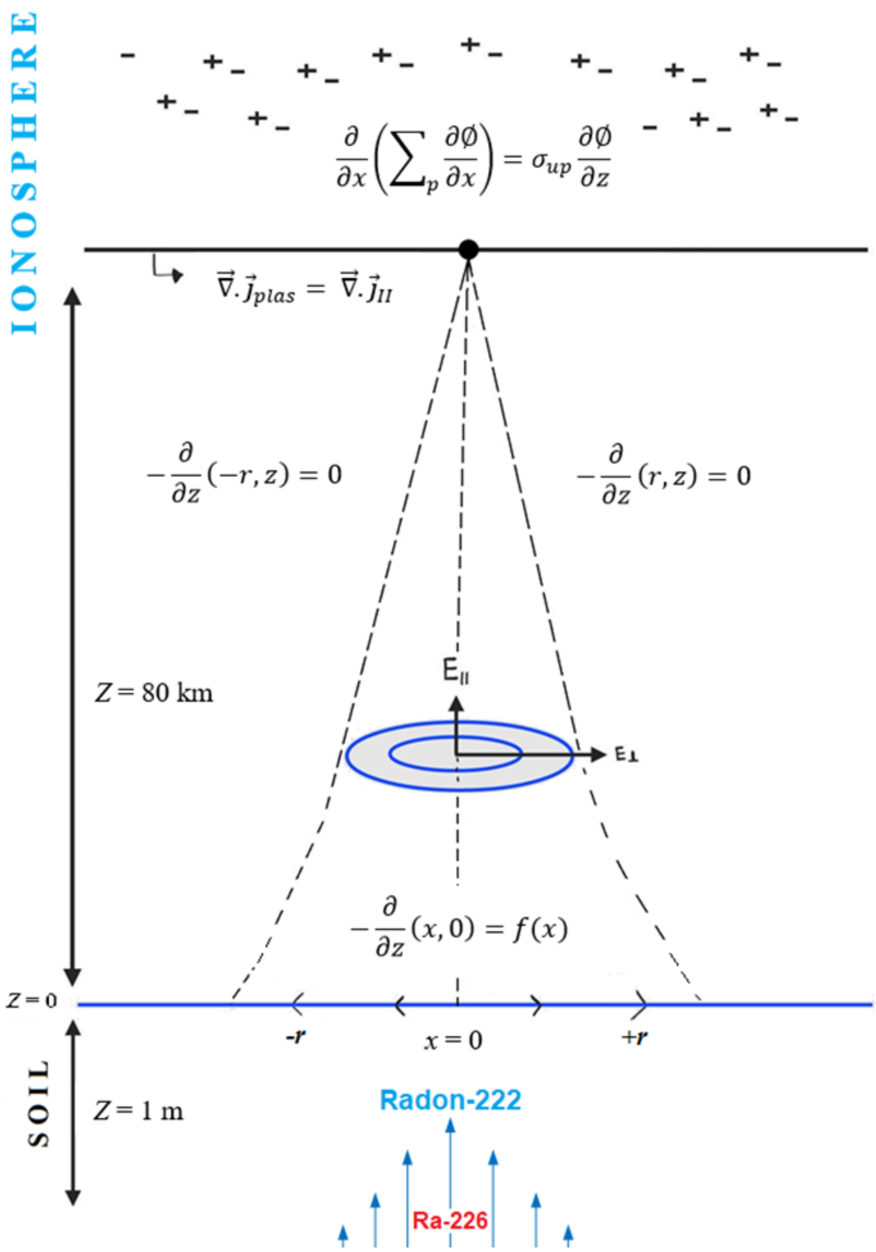

Figure 1: Lithosphere-Atmosphere-Ionosphere coupling schematic diagram. The effect of radon generated (due to earthquake) at 1m depth beneath the soil is estimated in the atmosphere, up to ionospheric heights (80 km). Boundary conditions which are based on the model assumptions are seen in the figure. The current reaching the ionospheric boundary layer is assumed to correlate with plasma electric field. The geomagnetic field is assumed to be parallel to the propagation of the electric field align *z*-axis.

2.3 Lower Boundary conditions

Beneath the soil surface above earthquake zone, the potential is expected to die out at far distances from the epicenter. i.e. let r be a point on x axis where a weaker influence of the potential is felt, then at a distance $x > r$, the potential should have a minimum or zero influence (Fig 1). In other words, $\phi(r, z) = \phi(-r, z) = 0$. This is important, because the relationship between the electric field reaching the ionosphere and the radius of influence r (or earthquake preparation radius) will be examined. The symmetry of $\cos(x)$, i.e. $\cos(-\theta) = \cos(\theta)$ makes it possible to preserve the function, resulting from Eq (6) to Eq (7b).

$$\phi(x,z) = \sum_{n=0}^{\infty} \cos(\sqrt{(\mu_n)}x)(A_n \exp(m_{1n}z) + B_n \exp(m_{2n}z)) \qquad (7b)$$

$\mu_n = \frac{\pi^2(2n-1)^2}{4r^2}$, $A_n = C_1C_3$, and $B_n = C_1C_4$. Another condition at the surface is that the potential ϕ satisfy Eq (8).

$$\frac{-\partial}{\partial z}\phi(-r,z) = \frac{-\partial}{\partial z}\phi(r,z) = 0 \qquad (8)$$

The epicenter $(x = 0, z = 0)$. This is where radon and its progeny are introduced to the atmosphere. In other words, the region of high ion production rates. It is where the local modification of atmospheric conductivity is pronounced. The electric field near the surface at $(0,0)$ is expected to have higher magnitudes compared to other distances. i.e. $\phi(x,z) < \phi(x = 0, z = 0)$, this is presented in Eq (9).

$$\frac{-\partial}{\partial z}\phi(x,0) = f(x) \qquad (9)$$

Eq (10) is chosen to represent the electric field behavior near the surface in the earthquake region for a given amplitude E_o. The choice of the function $f(x)$ depends on the desire to achieve a required symmetry or evenness in the interval $-x \le r \le x$. The reason for this is to simplify model formulation complexity. Models in literature carefully define $f(x)$ to achieve a desired symmetry, while satisfying the boundary conditions in the lower region of the LAIC model (Denisenko, et al., 2008; Denisenko et al., 2013; Khegai, 2020; Surkov et al., 2022; Xu et al., 2015a; Zhou et al., 2017). The left frame of Figure 2 presents a comparison between Eq (10), and some literature theoretical distributions for the near surface electric field. The graphs correspond to near surface values $E_o = 100\, V/m, r = 100km, -500km < x < 500km$. The right frame of Figure 2 depicts the derivatives of these functions, it is clear they all have similar behavior. The minor differences between the curves can lead to outcome variations in estimation processes. The functions in Figure 2 include $f(x) = E_o \exp(-x^2/r^2)$ (Surkov et al., 2022; Xu et al., 2015a), and $f(x) = E_o \cosh(\frac{2x}{r})$ (Denisenko, Boudjada, et al., 2008). Eq (10) performs well in observing symmetry while satisfying the boundary conditions. The function is also capable of restricting all values to exist within $-r \le x \le r$.

$$f(x) = \frac{E_o}{2}(1 + \cos(\frac{\pi x}{2r}))\exp(-x^2/r^2) \qquad (10)$$

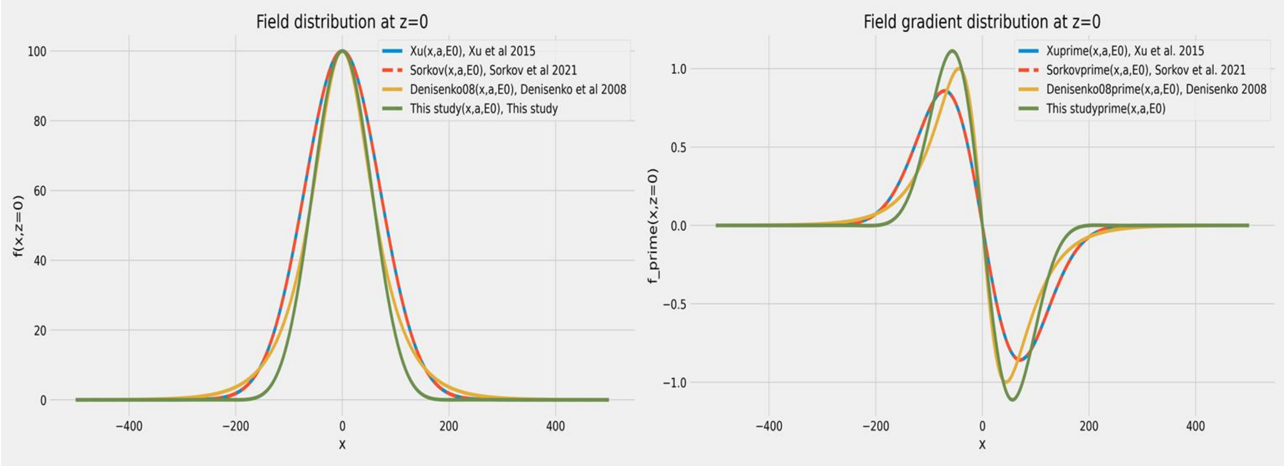

Figure 2: From the left, near surface electric field distribution, comparing Eq (10) with some theoretical models in literature. From the right is the gradient of these functions.

2.3.1 Radon transport

In earthquake periods, Rn gas can travel a long distance vertically from soil to atmosphere while ionizing its surroundings. A one-dimensional radon migration equation is presented in Eq (11) (Nazaroff, 1992).

$$\frac{\partial C_{Rn}}{\partial t} = D\frac{\partial^2 C_{Rn}}{\partial z^2} - u\frac{\partial C_{Rn}}{\partial z} - \lambda C_{Rn} + F \qquad (11)$$

F is the Rn production rate from its mother nuclei (Radium) $F = \lambda \epsilon C_{Ra}\rho$, λ is radon decay constant (s^{-1}), C_{Ra} in$(B_q m^{-3})$ is the radium concentration at a given time near the region of radon measurement, u is radon convective velocity in soil (ms^{-1}), D is the effective radon diffusion coefficient in soil $(m^2 s^{-1})$, z represent soil depth in meters (0-1 meter). ϵ is the radon emanation coefficient, it ranges between 0 and 1, and it is a measure of the effectiveness of soil in emitting radon gas. ρ is the soil bulk density (kgm^{-3}). Taking $z = 0$ at the soil surface (see Figure 1), and the migration assumed to flow upwards from a given soil depth (often at 1m). A solution with the boundary conditions presented in Eq (12) (Muhammad and Külahcı, 2022).

$$C_{Rn}(0,t) = f(t)(1-\alpha), \frac{(\partial C_{Rn}(z,t))}{(\partial z)}|_{z\to\infty} = 0 \qquad (12)$$

The function $f(t)$ in Eq (12), represents radon concentration recorded at a depth z and time t by the monitoring device, in this study the depth is 1meter. The constant α represents a fraction of radon that is attenuated during its journey from production depth to soil surface. With this in place, Eq (13) represents the radon migration model from production to surface.

$$C_{Rn}(z,t) = Q(1-\exp(-az)) + f(t)(1-\alpha)\exp(-az) \qquad (13)$$

where $a = -\frac{u}{2D} + \sqrt{\frac{u^2}{4D^2} - \frac{(w-\lambda)}{D}}$, and w is time evolution constant (s^{-1}), and $Q = \frac{F}{\lambda}$ represents radon concentration far from production point. The values $\alpha = 0.9952$, $a = 0.905$ are used in Eq (13) for soil to air Rn concentration estimations. The near surface electric field estimation is done for a quasi-stationary condition. To incorporate radon transport into to equations which follow, the time evolution constant $w = 0$, and Eq (13) becomes a steady state approximation to soil-air radon transport $C_{Rn}(z,t) \rightarrow C_{Rn}(z)$.

2.3.2 Lithosphere to Atmosphere ionization production

Radon decay products, such as bismuth and polonium, can ionize the air during seismic periods. This results in the creation of ion pairs and a net charge transfer between the Earth's atmosphere and the lithosphere (Harrison et al. 2017). The primary cause of this ion pair generation is the decay of polonium (^{218}Po and ^{214}Po), which releases alpha particles throughout its disintegration(Muhammad et al., 2024). By measuring the energy of the alpha particles produced by radon and its progeny and comparing it to the average energy required (35 eV) to create an ion-pair in the soil or in atmosphere, the ionization rate in soil or in air may be determined by using Eq (14) (Muhammad et al., 2021; Omori et al., 2007). Therefore, it is possible to estimate radon contribution to ion production rate $q(z)$ from soil to atmosphere by applying $C_{Rn}(z)$ of Eq (13) to Eq (14). This estimation is on the assumption that the contribution of other radon isotopes to ionization is small (due to short half-life) compared to that of ^{222}Rn.

$$q_{Rn}(z) = \frac{5.49\times10^{6} C_{Rn} + 6\times10^{6} C_{218Po} + 7.69\times10^{6} C_{214Po}}{35} \qquad (14)$$

A secular equilibrium between ^{214}Bi and ^{214}Po is also assumed in the implementation of Eq (14). The ratio of radon, polonium-218, and polonium-214 concentrations ($C_{Rn}, C_{218Po}, C_{214Po}$), averaged over time is found to be approximately 1:0.7:0.5 (Omori et al., 2007). Moreover, the attachment of these nuclides to aerosols does not affect the ionization of soil and atmosphere particles, as the range of alpha particles is much larger than the radius of the aerosols. The ratio 1:0.7:0.5 refers to the relative concentrations of three different nuclides (radon, polonium-218, and polonium-214) in a given sample. It means that for every 1 unit of radon, there are 0.7 units of polonium-218 and 0.5 units of polonium-214. This ratio is an average over time and assumes a secular equilibrium between ^{214}Bi and ^{214}Po.

2.5 Surface Electric field and conductivity (E_o, σ_o)

The atmospheric electric field generated in the near surface boundary layer (due to surface ionization) is assumed to have an amplitude, which is higher at the point where radon and its progeny are exhaled and decreases with distance from exhalation point. For a quasi-neutral atmosphere, the magnitude of radon induced atmospheric surface electric field E_o can be derived from the continuity equations for ions and aerosol particles, the equations of motion, and the Poisson equations for a given coordinate system. Shalimov and Riabova (2021) solved these equations using quasihydrodynamic assumptions to obtain the resulting near surface atmospheric electric field in one dimension along z-axis (Eq. (15)). Their simplification allows for a focused analysis of the system dynamics, disregarding horizontal variations and emphasizing the vertical dimension as the primary factor influencing the behavior of ions and aerosol particles.

$$E_o = \frac{eQ_a Z_a g}{2\sigma_o v_a} \qquad (15)$$

$e = 1.6023 \times 10^{-19}C$, $Q_a = 10C$ is aerosol particle charge(C), $g = 9.8ms^{-2}$. Z_a is the aerosol concentration (m^{-3}). The near surface atmospheric electric conductivity σ_o (Eq (16)) is defined in terms of charge mobility μ, ion concentration n, and the electric charge e. μ has a near surface value of about $(0.5 - 3.2) \times 10^{-4}m^2V^{-1}s^{-1}$(Anisimov et al., 2018; Omori et al., 2007; Rosen and Hofmann, 1981). The ion concentration also depends on the ion-ion recombination coefficient $\alpha = (1-3) \times 10^{-12}m^3s^{-1}$, the ion-aerosol attachment coefficient $\beta = (3-4) \times 10^{-12}m^3s^{-1}$, the ion production rate q, and the aerosol concentration Z_a (Eq. (17)) (Harrison et al., 2014; Rosen and Hofmann, 1981; Turbulent, 1983; Xu et al., 2015a)

$$\sigma_o \simeq 2\mu e n \qquad (16)$$

$$n = \frac{-\beta Z + \sqrt{(\beta Z_a)^2 + 4\alpha q}}{2\alpha} \qquad (17)$$

The parameter $v_a = \frac{9\eta}{2R_a^2\rho_a}$ in Eq. (15) denotes the effective collision frequency of aerosol particles; η is air viscosity $(1.8 \times 10^{-5}kgm^{-1}s^{-1})$, ρ_a is aerosol density, and R_a is the aerosol radius. The radius and density of aerosols can vary depending on the composition, size, and characteristics of the particles. $\rho_a = 2.5kgm^{-3}$ and $R_a = 1.2 \times 10^{-6}m$ are chosen for the estimation in this study. $Z_aQ_a = (10^6 - 10^{12})m^{-3}$ for near surface aerosols (Namgaladze et al., 2018).

3.0 Estimation Results

The general solution to Eq (6) using the boundary conditions Eqns 7a, 7b, 8, and 9 is given in Eq (15). Resulting atmospheric electric field components are determined using the relations in Eq (16). Estimated values for near surface electric parameters E_o, σ_o, ψ_o can be seen in the first four columns of Table 2. The last three columns contain estimated values for $E_z(0{,}80), \phi(0{,}80)$, and the surface ion production rate Q. These estimations are for the values $z_a = 10^9, \mu = 3 \times 10^{-4}m^3v^{-1}s^{-1}, \alpha = 10^{-12}m^3s^{-1}$, and $\beta = 4 \times 10^{-12}m^3s^{-1}$. Table 2 is structured such that; colored rows mark the start of new estimations (having repeated column names) for different Radon concentration Rn, and radius of influence r values. There are four sub tables in Table 2, one sub table for each of the elements in the sequence $r = \{399km, 199km, 19km, 1km\}$. For each value in r, estimations are made for radon concentrations.

$Rn = \{6.2\ kBqm^{-3}, 20.5\ kBqm^{-3}, 82.4\ kBqm^{-3}, 206\ kBqm^{-3}\}$ This can be seen in each of the sub tables.

$$\phi(x,z) = -\sum_n^{\infty} f(x) \frac{(\exp(m_{2n}z) - \lambda_n \exp(m_{1n}z))}{(m_{2n} - m_{1n}\lambda_n)} \quad (15)$$

where $$\lambda_n = \frac{\sigma_p \mu_n + \sigma(z_{up}) m_{2n}}{\sigma_p \mu_n + \sigma(z_{up}) m_{1n}} \exp((m_{2n} - m_{1n}) z_{up})$$

$$E_x = -\frac{\partial \phi}{\partial x} \text{ and } E_z = -\frac{\partial \phi}{\partial z} \quad (16)$$

According to estimation results, the near surface atmospheric electric field, and electric potential vary within the range $(1 - 27)\,V/m$ and $(0.3 - 162)\,V$ respectively (Table 2). The near surface conductivity varies within $(1 - 29) \times 10^{-14} Sm^{-1}$. The estimates are within a reasonable range (see Table 1 and (Pierce, 1976)). These electric field values are small compared to fair weather atmospheric electric field, which vary between 20 V/m to 220 V/m (Wu et al., 2023). However, such magnitudes can be significant when averaged over time due to continuous radon exhalation. In addition, it can be seen from Table 2 that, the boundary layer conductivity is more sensitive to radon exhalation compared to the electric field. This is due to its strong dependence on parameters such as aerosol concentration and ion production rate, and this makes it a potential candidate for detecting anomalies relative to atmospheric electric properties (Pierce, 1976). High surface conductivity implies that generated surface electric charges can move freely in the atmosphere. In regions with low conductivity, the charges will have a harder time moving through atmospheric layers. The relationship between atmospheric electric field, atmospheric conductivity, and ion production can be influenced by numerous factors such as meteorological conditions, geochemical properties of the region etc. For this reason, estimation results can vary depending on parameter configuration in the model. The important thing is to explore how these generated radon influences can reach ionospheric heights. Rn exhalation and the Ionosphere can both respond to lithospheric disturbances (e.g. earthquakes) (Park et al. 1997). However, the responses are not always correlated due to some physical processes (Muhammad et al., 2023). An interesting way to explain this indirect relationship is via the global electric circuit (Rycroft et al., 2000; Sorokin and Ruzhin, 2015). There could be two possible ways here. First is when radon influence is favored by atmospheric conditions (e.g. vertical convective currents) to reach ionospheric heights. The second is the modification of conductive current between earth and ionosphere. Charges generated by exhaled radon and its progeny from the lithosphere can affect the boundary layer conductivity (Table 2). The locality within the radius of influence r becomes quasi-ionized. Perturbation in the vertical or horizontal direction induces an electromotive force (EMF), which decreases with height. An EMF current is generated within the localized exhalation region (extraneous current). The vertical and horizontal components of this current depend on physical atmospheric processes such as winds, air masses, convective currents, and jet streams. The uplift and gravitational settling of charges in vertical direction would be a major source of this extraneous current. This is because, under atmospheric thermal instability conditions (e.g. earthquake influences), atmospheric ions and aerosols are transported by turbulent eddies. These eddies move the ions and aerosols from regions of high concentration at higher altitudes to areas of lower concentration. A state of equilibrium is attained when the vertical aerosol movement is counteracted by gravitational settling (Sorokin and Ruzhin, 2015). This effect, when added to the conductive current, can cause variations in locality of the GEC system. It is possible to estimate the magnitude of this radon induced extraneous current right above the Earth's surface from Eq (16) and Eq (19). Using Ohm's law, this current can be of the order $(10^{-12} - 10^{-13})Am^{-1}$. This current is also low when compared to fair weather GEC current $j \approx 10^{-9}Am^{-2}$ (Daskalopoulou et al., 2021; Kudintseva et al., 2016; Xu et al., 2015b). However, it is comparable with the near surface current estimations due to Sahara dust by (Daskalopoulou et al., 2021). This is another implication of chosen model parameters as mentioned earlier.

According to Figure 3, the behavior of E_z and the potential $\phi(x,z)$ vary independent of height. They both have higher magnitudes at the origin and decrease with increase in distance from the origin at any given height. This behavior can be attributed to the non-stratified nature of the conductivity profile, as well as the influence of $f(x)$ in Eq(10). As seen in Figure 3, the magnitudes of E_z and $\phi(x,z)$ are dominant in lower altitudes ($(z < 20km)$). At these heights, the atmosphere is dominated by about 78% Nitrogen, and 21% Oxygen. About 99% of Earth's water vapor also exists within this region, and Radon influence (ionization) is favored. Beyond this, the concentration of these gasses drastically decreases, and radon influence is seen to decline. At ionospheric heights (80 km), about 99.9999% of these magnitudes are already gone, resulting to $E_{zup} \sim 10^{-5}\,V/m$ and $\phi(x,z) \sim 10^{-7}V$. This is expected because, radon ionization effects are dominant in some few meters above Earth's surface. It is possible to look at these estimation results by assuming that the radius of influence r is comparable to earthquake preparation radius (Dobrovolsky et al., 1979). Fleischer (1981) presented an empirical relation for earthquakes of various magnitudes; $r = 10^{0.43M}, M \geq 3$ and $r = \frac{10^{0.813M}}{16.6}, M < 3$ (Deb et al., 2018).

Table 2: Estimated values for near surface electric parameters E_o, σ_o, ψ_o.

r =399.00km	1m soil $Rn(Bqm^{-3})$	$E_0(v/m)$	$\phi_o(v)$	$\sigma_o(S/m)$	$E_{up}(v/m)$	$\phi_{up}(v)$	Q (m^{-3})
Rn=30 Bq/m3	6.20E+03	1.12E+01	6.70E+01	3.26E-14	1.80E-05	2.33E-07	1.16E+07
Rn=99Bq/m3	2.05E+04	4.84E+00	2.90E+01	7.52E-14	7.78E-06	2.33E-07	3.83E+07
Rn=399Bq/m3	8.24E+04	2.06E+00	1.23E+01	1.77E-13	3.31E-06	2.33E-07	1.54E+08

Rn=999Bq/m3	2.06E+05	1.23E+00	7.35E+00	2.97E-13	1.97E-06	2.33E-07	3.86E+08
r =199.00km	**1m soil** $Rn(Bqm^{-3})$	$E_0(v/m)$	$\phi_o(v)$	$\sigma_o(S/m)$	$E_{up}(v/m)$	$\phi_{up}(v)$	Q (m^{-3})
Rn=10Bq/m3	2.07E+03	2.71E+01	1.62E+02	1.34E-14	4.26E-05	5.68E-08	3.87E+06
Rn=30Bq/m3	6.20E+03	1.12E+01	6.69E+01	3.26E-14	1.76E-05	5.68E-08	1.16E+07
Rn=99Bq/m3	2.05E+04	4.84E+00	2.90E+01	7.52E-14	7.62E-06	5.68E-08	3.83E+07
Rn=399Bq/m3	8.24E+04	2.06E+00	1.23E+01	1.77E-13	3.24E-06	5.68E-08	1.54E+08
Rn=999Bq/m3	2.06E+05	1.23E+00	7.34E+00	2.97E-13	1.93E-06	5.68E-08	3.86E+08
r =19.00km	**1m soil** $Rn(Bqm^{-3})$	$E_0(v/m)$	$\phi_o(v)$	$\sigma_o(S/m)$	$E_{up}(v/m)$	$\phi_{up}(v)$	Q (m^{-3})
Rn=10Bq/m3	2.07E+03	2.71E+01	1.35E+02	1.34E-14	3.36E-06	4.08E-11	3.87E+06
Rn=30Bq/m3	6.20E+03	1.12E+01	5.56E+01	3.26E-14	1.39E-06	4.08E-11	1.16E+07
Rn=99Bq/m3	2.05E+04	4.84E+00	2.41E+01	7.52E-14	6.01E-07	4.08E-11	3.83E+07
Rn=399Bq/m3	8.24E+04	2.06E+00	1.03E+01	1.77E-13	2.56E-07	4.08E-11	1.54E+08
Rn=999Bq/m3	2.06E+05	1.23E+00	6.11E+00	2.97E-13	1.52E-07	4.08E-11	3.86E+08
r =9.00km	**1m soil** $Rn(Bqm^{-3})$	$E_0(v/m)$	$\phi_o(v)$	$\sigma_o(S/m)$	$E_{up}(v/m)$	$\phi_{up}(v)$	Q (m^{-3})
Rn=10Bq/m3	2.07E+03	2.71E+01	9.78E+01	1.34E-14	9.18E-09	2.50E-14	3.87E+06
Rn=30Bq/m3	6.20E+03	1.12E+01	4.04E+01	3.26E-14	3.79E-09	2.50E-14	1.16E+07
Rn=99Bq/m3	2.05E+04	4.84E+00	1.75E+01	7.52E-14	1.64E-09	2.50E-14	3.83E+07
Rn=399Bq/m3	8.24E+04	2.06E+00	7.44E+00	1.77E-13	6.98E-10	2.50E-14	1.54E+08
Rn=999Bq/m3	2.06E+05	1.23E+00	4.43E+00	2.97E-13	4.16E-10	2.50E-14	3.86E+08
r =1.00km	**1m soil** $Rn(Bqm^{-3})$	$E_0(v/m)$	$\phi_o(v)$	$\sigma_o(S/m)$	$E_{up}(v/m)$	$\phi_{up}(v)$	Q (m^{-3})
Rn=10Bq/m3	2.07E+03	2.71E+01	1.63E+01	1.34E-14	1.46E-56	4.90E-64	3.87E+06
Rn=30Bq/m3	6.20E+03	1.12E+01	6.74E+00	3.26E-14	6.02E-57	4.90E-64	1.16E+07
Rn=99Bq/m3	2.05E+04	4.84E+00	2.92E+00	7.52E-14	2.61E-57	4.90E-64	3.83E+07
Rn=399Bq/m3	8.24E+04	2.06E+00	1.24E+00	1.77E-13	1.11E-57	4.90E-64	1.54E+08
Rn=999Bq/m3	2.06E+05	1.23E+00	7.40E-01	2.97E-13	6.61E-58	4.90E-64	3.86E+08
r =0.50km	**1m soil** $Rn(Bqm^{-3})$	$E_0(v/m)$	$\phi_o(v)$	$\sigma_o(S/m)$	$E_{up}(v/m)$	$\phi_{up}(v)$	Q (m^{-3})
Rn=10Bq/m3	2.07E+03	2.71E+01	8.39E+00	1.34E-14	4.35E-111	3.66E-119	3.87E+06
Rn=30Bq/m3	6.20E+03	1.12E+01	3.46E+00	3.26E-14	1.79E-111	3.66E-119	1.16E+07
Rn=99Bq/m3	2.05E+04	4.84E+00	1.50E+00	7.52E-14	7.77E-112	3.66E-119	3.83E+07
Rn=399Bq/m3	8.24E+04	2.06E+00	6.38E-01	1.77E-13	3.31E-112	3.66E-119	1.54E+08
Rn=999Bq/m3	2.06E+05	1.23E+00	3.80E-01	2.97E-13	1.97E-112	3.66E-119	3.86E+08

For the first two sub tables (in Table 2), the theoretical earthquake magnitudes corresponding to 399.00 km and 199.00 km preparation radii are 6 and 5.34 (Richter scale), respectively. The near surface estimated variables due to these earthquakes are seen in the first and second sub-tables in Table2. The radon induced electric field and electric potential at ionospheric heights are both of the order of $10^{-6}V/m$. These estimation outcomes are for the assumption that, radon and its progeny are the source of lower atmospheric properties in the disturbed (earthquake) region. In addition, the values are comparable to estimations presented in Table 1. In this regard, it is possible to infer that, the relationship between radon ionization and atmospheric electric properties has profound implications, as it suggests that radon-induced changes in atmospheric conductivity might serve as an early indicator, or a diagnostic tool, to detect anomalies in the atmospheric electric properties.

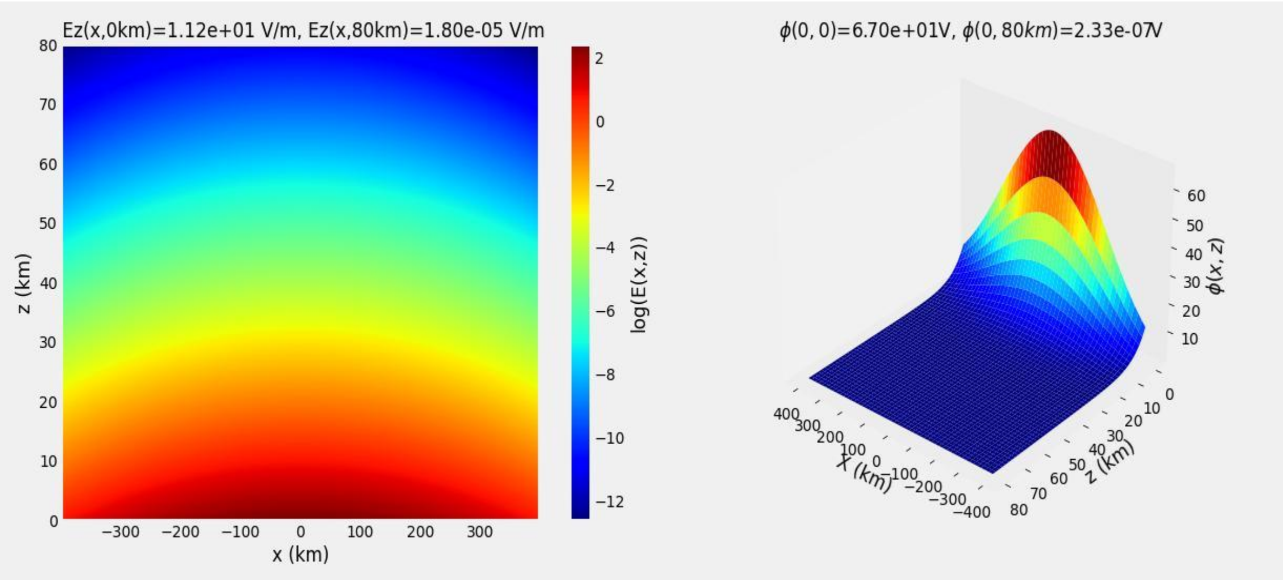

Figure 3: Electric field E_z (x, z) and electric potential Φ(x, z) behavior from the ground to the ionosphere

The discussion has so far focused on radon influence in atmosphere due to seismic effects. However, it is also possible to explore the model outcomes under non-seismic conditions. This can be achieved by analyzing model outcomes under different fair-weather conditions. For example, the variation of parameters like ion-aerosol attachment rates relative to non-seismic conditions can result in different model outcomes. In this case, radon variation also needs to be relative to the fair whether values. A major limitation of studies like the one presented in this article is that the assumptions made in the process of modeling often affect its accuracy. For example, herein, meteorological factors like soil/atmospheric temperature and pressure were not incorporated. These factors are significant for both radon and the atmospheric processes. However, for simplicity, with the steady state condition, such effects are minimal. In order to properly explore the model presented herein, simultaneous Radon, atmospheric, and Ionospheric measurements are required. This is challenging, as some of these parameters (e.g. recombination rate) are quite difficult to monitor. Nevertheless, the authors look forward to collaborating with experimentalist in the future to determine these consequences.

Conclusions

This research provides a comprehensive mathematical and empirical analysis of the influence of radon-induced ionization on atmospheric electric fields and potentials, with significant implications for earthquake monitoring. The findings indicate that boundary layer conductivity is more sensitive to radon exhalation compared to the electric field, and that local atmospheric conditions can significantly affect the transport and impact of radon-induced ions. The study suggests a potential connection between radon emanations and seismic activities, which could offer new insights into earthquake precursors and disaster prediction. The tabulated reference values and radial behavior of electric parameters offer valuable tools for future observational studies aimed at disaster preparedness. Overall, this work contributes to a deeper understanding of the complex interactions between lithospheric radon exhalation and atmospheric and ionospheric electric properties, highlighting the importance of integrating observational datasets and real-world measurements to advance our knowledge in earthquake prediction and disaster management.

Acknowledgments

We would like to thank ASELSAN, Batman and Qatar University for supplying a suitable environment for the research.

Author declaration

We wish to confirm that there are no known conflicts of interest associated with this publication and there has been no significant financial support for this work that could have influenced its outcome. We confirm that we have given due consideration to the protection of intellectual property associated with this work and that there are no impediments to publication, including the timing of publication, with respect to intellectual property. In so doing we confirm that we have followed the regulations of our institutions concerning intellectual property.

References

Anisimov, S. V., Galichenko, S. V., Aphinogenov, K. V., and Prokhorchuk, A. A. (2018). Evaluation of the Atmospheric Boundary-Layer Electrical Variability. *Boundary-Layer Meteorology*, *167*(2), 327–348. https://doi.org/10.1007/s10546-017-0328-0

Chree, C. (1913). Some phenomena of sunspots and of terrestrial magnetism at Kew Observatory. Journal of Geophysical Research, 18(1), 120-151.

Daskalopoulou, V., Mallios, S. A., Ulanowski, Z., Hloupis, G., Gialitaki, A., Tsikoudi, I., et al. (2021). The electrical activity of Saharan dust as perceived from surface electric field observations. *Atmospheric Chemistry and Physics*, *21*(2), 927–949. https://doi.org/10.5194/acp-21-927-2021

Deb, A., Gazi, M., Ghosh, J., Chowdhury, S., and Barman, C. (2018). Monitoring of soil radon by SSNTD in Eastern India in search of possible earthquake precursor. *Journal of Environmental Radioactivity*, *184–185*(January), 63–70. https://doi.org/10.1016/j.jenvrad.2018.01.009

Denisenko, V. V., Boudjada, M. Y., Horn, M., Pomozov, E. V., Biernat, H. K., Schwingenschuh, K., et al. (2008). Ionospheric conductivity effects on electrostatic field penetration into the ionosphere. *Natural Hazards and Earth System Science*, *8*(5), 1009–1017. https://doi.org/10.5194/nhess-8-1009-2008

Denisenko, V. V., Biernat, H. K., Mezentsev, A. V., Shaidurov, V. A., and Zamay, S. S. (2008). Modification of conductivity due to acceleration of the ionospheric medium. *Annales Geophysicae*, *26*(8), 2111–2130. https://doi.org/10.5194/angeo-26-2111-2008

Denisenko, V. V., Ampferer, M., Pomozov, E. V., Kitaev, A. V., Hausleitner, W., Stangl, G., and Biernat, H. K. (2013). On electric field penetration from ground into the ionosphere. *Journal of Atmospheric and Solar-Terrestrial Physics*, *102*, 341–353. https://doi.org/10.1016/j.jastp.2013.05.019

Denisenko, Valery, Rycroft, M., and Harrison, R. G. (2019). A Mathematical Model of the Ionospheric Electric Field Which Closes the Global Electric Circuit. *Springer Proceedings in Earth and Environmental Sciences*, 455–463. https://doi.org/10.1007/978-3-030-31970-0_48

Dobrovolsky, I. P., Zubkov, S. I., and Miachkin, V. I. (1979). Estimation of the size of earthquake preparation zones. *Pure and Applied Geophysics PAGEOPH*, *117*(5), 1025–1044. https://doi.org/10.1007/BF00876083

Harrison, R. G., Aplin, K. L., and Rycroft, M. J. (2014). Brief Communication: Earthquake-cloud coupling through the global atmospheric electric circuit. *Natural Hazards and Earth System Sciences*, *14*(4), 773–777. https://doi.org/10.5194/nhess-14-773-2014

Harrison, R. G., Nicoll, K. A., and Aplin, K. L. (2017). Evaluating stratiform cloud base charge remotely. Geophysical Research Letters, 44(11), 5702-5708).

Khegai, V. V. (2020). Analytical Model of a Seismogenic Electric Field According to Data of Measurements in the Surface Layer of the Midlatitude Atmosphere and Calculation of Its Magnitude at the Ionospheric Level. *Geomagnetism and Aeronomy*, *60*(4), 507–520. https://doi.org/10.1134/S0016793220030081

Kudintseva, I. G., Nickolaenko, A. P., Rycroft, M. J., and Odzimek, A. (2016). AC and DC global electric circuit properties and the height profile of atmospheric conductivity. *Annals of Geophysics*, *59*(5). https://doi.org/10.4401/ag-6870

Märcz, F. (1997). The atmospheric electric field and radon: Observations at Nagycenk, Hungary.

Journal of Geophysical Research: Atmospheres, 102(D9), 10983-10992.

Muhammad, A., and Külahcı, F. (2022). Radon transport from soil to air and Monte-Carlo simulation. *Journal of Atmospheric and Solar-Terrestrial Physics*, *227*, 105803. https://doi.org/10.1016/j.jastp.2021.105803

Muhammad, A., Külahcı, F., Salh, H., and Hama Rashid, P. A. (2021). Long Short Term Memory networks (LSTM)-Monte-Carlo simulation of soil ionization using radon. *Journal of Atmospheric and Solar-Terrestrial Physics*, *221*, 105688. https://doi.org/10.1016/j.jastp.2021.105688

Muhammad, A., Külahcı, F., and Birel, S. (2023). Investigating radon and TEC anomalies relative to earthquakes via AI models. *Journal of Atmospheric and Solar-Terrestrial Physics*, *245*, 106037. https://doi.org/10.1016/j.jastp.2023.106037

Namgaladze, A., Karpov, M., and Knyazeva, M. (2018). Aerosols and seismo-ionosphere coupling: A review. *Journal of Atmospheric and Solar-Terrestrial Physics*, *171*(February), 83–93. https://doi.org/10.1016/j.jastp.2018.01.014

Nazaroff, W. W. (1992). Radon transport from soil to air. *Reviews of Geophysics*, *30*(2), 137–160. https://doi.org/10.1029/92RG00055

Omori, Y., Yasuoka, Y., Nagahama, H., Kawada, Y., Ishikawa, T., Tokonami, S., and Shinogi, M. (2007). Anomalous radon emanation linked to preseismic electromagnetic phenomena. *Natural Hazards and Earth System Science*, *7*(5), 629–635. https://doi.org/10.5194/nhess-7-629-2007

Park, S., Moraal, H., and Stoker, P. H. (1997). Radon as an earthquake precursor. Journal of Geophysical Research: Space Physics, 102(A7), 14,201-14,209.

Pierce, E. T. (1976). Atmospheric electricity and earthquake prediction. *Geophysical Research Letters*, *3*(3), 185–188. https://doi.org/10.1029/GL003i003p00185

Prokhorov, B. E., and Zolotov, O. V. (2017). Comment on “An improved coupling model for the lithosphere-atmosphere-ionosphere system” by Kuo et al. [2014]. *Journal of Geophysical Research: Space Physics*, *122*(4), 4865–4868. https://doi.org/10.1002/2016JA023441

Prokhorov, Boris E., Zolotov, O. V., Knyazeva, M. A., and Romanovskaya, Y. V. (2019). Simulated vertical electric field data: An estimation from an improved coupling model for the lithosphere-atmosphere-ionosphere system. *Data in Brief*, *26*, 104513. https://doi.org/10.1016/j.dib.2019.104513

Rosen, J. M., and Hofmann, D. J. (1981). Balloon-borne measurements of electrical conductivity, mobility, and the recombination coefficient. *Journal of Geophysical Research*, *86*(C8), 7406. https://doi.org/10.1029/jc086ic08p07406

Rycroft, M. J., Israelsson, S., and Price, C. (2000). The global atmospheric electric circuit, solar activity and climate change. Journal of Atmospheric and Solar-Terrestrial Physics, 62(17-18), 1563-1576.

Shalimov, S. L., and Riabova, S. A. (2021). A Possible Mechanism of Variations in the Electric Field of the Surface Atmosphere during Strong Remote Earthquakes. *Doklady Earth Sciences*, *499*(2), 666–669. https://doi.org/10.1134/S1028334X21080146

Sorokin, V. M., and Ruzhin, Y. Y. (2015). Electrodynamic model of atmospheric and ionospheric processes on the eve of an earthquake. *Geomagnetism and Aeronomy*, *55*(5), 626–642. https://doi.org/10.1134/S0016793215050163

Sorokin, V. M., and Yaschenko, A. K. (2000). Electric field disturbance in the earth - ionosphere layer. *Advances in Space Research*, *26*(8), 1219–1223. https://doi.org/10.1016/S0273-1177(99)01221-1

Sorokin, Valery M., Chmyrev, V. M., Hayakawa, M., Sorokin, V. M., Chmyrev, V. M., and Hayakawa, M. (2020). A Review on Electrodynamic Influence of Atmospheric Processes to the Ionosphere.

Open Journal of Earthquake Research, *9*(2), 113–141. https://doi.org/10.4236/OJER.2020.92008

Surkov, V. V., Pilipenko, V. A., and Silina, A. S. (2022). Can Radioactive Emanations in a Seismically Active Region Affect Atmospheric Electricity and the Ionosphere? *Izvestiya, Physics of the Solid Earth*, *58*(3), 297–305. https://doi.org/10.1134/S1069351322030090

Turbulent, T. (1983). by Interfacial Ion Transfer, *88*, 8453–8469.

Wu, J., Zou, Z., Chen, T., Li, Y., Lu, Y., Ti, S., and Li, L. (2023). Diurnal variation of the fair-weather atmospheric electric field in Binchuan, China. *Journal of Atmospheric and Solar-Terrestrial Physics*, *242*(1), 105985. https://doi.org/10.1016/j.jastp.2022.105985

Xu, T., Zhang, H., Hu, Y., and Wu, J. (2015a). Electric field penetration into the ionosphere in the presence of anomalous radon emanation. *Advances in Space Research*, *55*(12), 2883–2888. https://doi.org/10.1016/j.asr.2015.03.015

Xu, T., Zhang, H., Hu, Y., and Wu, J. (2015b). Electric field penetration into the ionosphere in the presence of anomalous radon emanation. *Advances in Space Research*, *55*(12), 2883–2888. https://doi.org/10.1016/j.asr.2015.03.015

Zhou, C., Liu, Y., Zhao, S., Liu, J., Zhang, X., Huang, J., et al. (2017). An electric field penetration model for seismo-ionospheric research. *Advances in Space Research*, *60*(10), 2217–2232. https://doi.org/10.1016/j.asr.2017.08.007

Engineering, E. (2018). *Developments in Earthquake Geotechnics* (Vol. 43). http://link.springer.com/10.1007/978-3-319-62069-5

Ersoy, Ş., & Koçak, A. (2016). Disasters and earthquake preparedness of children and schools in Istanbul, Turkey. *Geomatics, Natural Hazards and Risk*, *7*(4), 1307–1336. https://doi.org/10.1080/19475705.2015.1060637

Havemann, S., Liu, J., Zhang, X., Yang, X., Yang, M., Zhang, T., Bao, Z., Wu, W., Qiu, G., Yang, X., & Lu, Q. (2023). *The Analysis of Lithosphere-Atmosphere-Ionosphere Coupling Associated with the 2022 Luding Ms6.8 Earthquake*. https://doi.org/10.3390/rs15164042

Kanamori, H. (1972). Mechanism of tsunami earthquakes. *Physics of the Earth and Planetary Interiors*, *6*(5), 346–359. https://doi.org/10.1016/0031-9201(72)90058-1

Mohammed, D. H. K., Külahcı, F., & Muhammed, A. (2021). Determination of possible responses of Radon-222, magnetic effects, and total electron content to earthquakes on the North Anatolian Fault Zone, Turkiye: an ARIMA and Monte Carlo Simulation. *Natural Hazards*, *108*(3), 2493–2512. https://doi.org/10.1007/s11069-021-04785-8

Muhammad, A., Külahcı, F., & Akram, P. (2020). Modeling radon time series on the North Anatolian Fault Zone, Turkiye: Fourier transforms and Monte Carlo simulations. *Natural Hazards*, *104*(1), 979–996. https://doi.org/10.1007/s11069-020-04200-8

Muhammad, A., Külahcı, F., & Birel, S. (2023). Investigating radon and TEC anomalies relative to earthquakes via AI models. *Journal of Atmospheric and Solar-Terrestrial Physics*, *245*, 106037. https://doi.org/10.1016/j.jastp.2023.106037

Muhammad, A., Külahcı, F., & Danbatta, S. J. (2024). Ion Transport from Soil to Air and Electric Field Amplitude of the Boundary Layer. *Geomagnetism and Aeronomy*, *64*(4), 581–591. https://doi.org/10.1134/S0016793223600613

Pulinets, S. A., Alekseev, V. A., Boyarchuk, K. A., Hegai, V. V., & Depuev, V. K. H. (1999). Radon and ionosphere monitoring as a means for strong: Earthquakes forecast. *Nuovo Cimento Della Societa Italiana Di Fisica C*, *22*(3–4), 621–626.

Sorokin, V., & Hayakawa, M. (2013). Generation of seismic-related DC electric fields and lithosphere-atmosphere-ionosphere coupling. *Modern Applied Science*, *7*(6), 1–25. https://doi.org/10.5539/mas.v7n6p1

Walter, T. R., & Amelung, F. (2006). Volcano‐earthquake interaction at Mauna Loa volcano, Hawaii. *J. Geophys. Res*, *111*, 5204. https://doi.org/10.1029/2005JB003861